IEEE Access
Multidisciplinary ⋮ Rapid Review ⋮ Open Access Journal

Received December 18, 2019, accepted January 15, 2020, date of publication February 11, 2020, date of current version February 18, 2020.

Digital Object Identifier 10.1109/ACCESS.2020.2971711

Ocean Wave Buoy Based on Parallel Six-Dimensional Accelerometer

YUNPING LIU[1], XIN WANG[1], JINGJING YOU[2], AND CHENG CHEN[3]

[1]Jiangsu Province Atmospheric Environment and Equipment Technology Collaborative Innovation Center, Nanjing University of Information Science and Technology, Nanjing 210044, China
[2]College of Mechanical and Electronic Engineering, Nanjing Forestry University, Nanjing 210037, China
[3]Nanjing Automation Institute of Water Conservancy and Hydrology, Nanjing 210012, China

Corresponding authors: Yunping Liu (liuyunping@nuiste.edu.cn) and Jingjing You (youjingjing251010@126.com)

This work was supported in part by the Natural Science Foundation of China under Grant 51875293, and in part by the National Key Research and Development Program of China under Grant 2018YFC1405703.

ABSTRACT Ocean wave parameters, including wave height, direction and period, are necessary to improve forecasts of ocean wave conditions. Their accurate observation contributes to safety of both offshore operations and military operations. However, conventional wave observation methods that combine the three-axis accelerometer-based wave sensor with the gyroscope may show problems such as inner arm error, transverse sensitivity effect, and gyroscope drift. The first two are due to non-coincidence of centroids inside the accelerometer. Such problems will reduce reliability of data. To solve the problems, a new type of parallel six-dimensional accelerometer is developed to reduce principle errors and improve stability of wave buoys. The solution features a single mass and 12-chain redundancy. When compared with the performance of high-precision sensors in the wave pool, the wave buoy based on six-dimensional accelerometer is proved to be more accurate in wave height measurement than 3.75 % $\times$ measurement value, with wave direction accuracy of $\pm$ 1°, and the wave period measurement accuracy of $\pm$ 0.1s.

INDEX TERMS Ocean wave sensor, parallel structure, high precision, wave buoys.

I. INTRODUCTION

Ocean wave characteristics, including wave height, direction and period, are vital for ocean development, waterborne transport, national defense and marine disaster prevention, so it is highly valued by marine scientific research [1]. There are many kinds of wave observation methods, such as manual measurement, instrumental measurement and remote sensing inversion measurement [2], but each method has its limitations. The accuracy of manual measurement is general, the continuity is poor, and its observation results have human errors. Instrumental measurement methods, such as the wave measuring rod [3], pressure-type [4], [5] and acoustic wave measurement [6], [7], cannot measure the wave direction, and are easy to be affected by environmental factors and measuring devices. The accuracy of remote sensing inversion (such as radar [8] and satellite altimeter measurement [9], [10]) is poor and the devices are very expensive. However, the wave buoy using accelerometers in this paper has high accuracy in observation methods [2]. Moreover, it is not affected by the space-time range and has a wide range of observation periods. Since its appearance, it has been the main mean of ocean wave observation [11].

There are two current methods of buoy wave measurement based on accelerometers, one is based on gravity accelerometer, and the other is based on three-axis accelerometer [12]. The first method uses a vertical accelerometer and a tilt sensor to measure the accelerations in the vertical direction and the azimuth angle of the buoy tilt respectively. After data processing, the wave height, wave period, and wave direction are obtained. Representative products include the US ENDECO/YSI 1156 wave direction trajectory buoy [13], the Dutch Datawell company's wave knight Directional Waverider MKIII [14], [15], the Norwegian Fugrooeeanor wavescan buoy [16] and the Chinese SZF wave buoy [17], [18]. The Directional waverider MKIII measures the wave height by an accelerometer and wave direction by combining the horizontal accelerometer with an electronic compass, thus forming a complete sensor unit.

The second method estimates the wave characteristics by measuring the accelerations on three axes and rotation angles (heading angle, pitch angle and roll angle)

The associate editor coordinating the review of this manuscript and approving it for publication was Usama Mir.

This work is licensed under a Creative Commons Attribution 4.0 License. For more information, see http://creativecommons.org/licenses/by/4.0/

of the buoy, such as the AXYS TRIAXYS Directional Wave Buoy [19], [20]. TRIAXYS Directional Wave Buoy consists of three accelerometers (three sensors are placed orthogonal), three gyroscopes, and an electronic compass. It provides continuous wave sampling of six parameters (X, Y, Z-axis acceleration and dip), under the motion of 8 Hz. A PC-104 microprocessor in the buoy could take samples, process data, and store information at the same time. Processed wave data files are logged onto a PCMCIA Flash RAM. The on-board data processor uses a special iterative algorithm developed by the Canadian Hydraulics Centre (CHC) of the National Research Council of Canada (NRC) for time-domain analysis and frequency-domain spectrum analysis. The values of wave height, average wave height, maximum wave height, effective wave period, effective wave height at spectrum analysis m_0 (m_0 is the zero moment of wave spectrum) time, spectral analysis of all frequencies (mean wave periods), spectral analysis of peak wave period and time-domain/frequency-domain parameters could be well obtained. Compared with the wave measurement of a single accelerometer, the combination of three accelerometers and gyroscopes can better reflect the movement track of the buoy in three-dimensional space, and can measure the inclination angles to get more accurate displacement information [21].

However, the accuracy of three single-axis accelerometers in conventional wave buoys was often affected due to uneven positions (X, Y, and Z planes) and inconsistent starting points of the units. In addition, lever-arm effect and lateral sensitivity error also increased the measurement errors, which inevitably accumulated and magnified after two integrations. Gyroscope drift also diminished the accuracy. It is necessary to improve the wave sensor unit. Early studies focused on three-dimensional linear accelerometers. K. Okada developed a piezoelectric tri-axial accelerometer [22], and successfully measured three-dimensional linear accelerations. The 3355 three-dimensional accelerometer [23] designed by EG&G placed three independent sensor units in three sensitive directions orthogonally. Its principle was similar to that of the TRIAXYS Wave Buoy, and measurement errors occurred due to the inconsistency of centroids of three sensors. Takao *et al.* [24] designed a micromechanical, piezoresistive three-dimensional accelerometer, using an integrated multidimensional sensor scheme. By sharing a mass in each sensitive direction of the accelerometer, both sensitivity and accuracy were improved, but its dimensional coupling degree was large.

There was little research on angular accelerometers. With the assistance of Teledyne Company, JAXA (Japan Aerospace Exploration Agency) developed a three-axis angular accelerometer [25], which successfully detected three angular accelerations of aircraft.In order to solve the problems such as large volume, high cost, and low precision in measuring six-dimensional accelerations by using the ''accelerometers + gyroscopes'' method, six-dimensional accelerometers began to develop. For example, Draper Lab and Rockwell International Corporation jointly designed an inertial sensor including three micro gyroscopes and three micro accelerometers [26]. Wang and Yuan [27] proposed a six-dimensional accelerometer based on a coplanar combination of six-degree-of-freedom accelerometers. Wang and Yuan [28] proposed a ''low cost, gyro-free, simple mass'' accelerometer. Li *et al.* [29] and You [30] designed a six-dimensional accelerometer based on 9-chain, but this scheme had the disadvantages of output signals distortion and lack of real-time due to structural limitations and generalized momentum. Six-dimensional accelerometers have developed rapidly, but most of them have narrow operating frequency band and low precision [31], which cannot meet the requirements of measuring waves (ocean waves have strong randomness in frequency and are mostly low-frequency waves near the coast). Therefore, there is no report on applying six-dimensional accelerometers to wave buoys currently.

To deal with these problems, this paper has designed a new 12-chain parallel accelerometer for the monitoring of wave accelerations. The main advantages of applying the six-dimensional accelerometer on wave buoy are as follows:

(1) In this paper, the parallel six-dimensional accelerometer is used as the acquisition unit. It is designed as a tetrahedral redundant parallel structure with single mass. The design has a compact topological structure, good decoupling property, wide operating frequency band, and low processing cost, avoids the lever arm effect and lateral sensitivity effect of the combination of three accelerometers. Besides, it improves the measurement accuracy.

(2) According to the piezoelectric theory, the deformations of 12 branches are inversed and calculated. Next, the motion amount of the inertial mass relative to the shell is calculated by using the kinematics theory of the parallel structure, and the motion amount of the mass relative to the inertial coordinate system is deduced. Finally, six parameters (three line accelerations and three angular accelerations on the X, Y, and Z axes) are calculated by dynamic modeling and decoupling algorithm. The decoupling algorithm has the characteristics of strong universality, high precision and good real-time performance.

(3) The sensor adopts a gyroscope-free design, which avoids the problem of zero drift error when the conventional buoy uses gyroscopes.

The parallel six-dimensional accelerometer in this paper could well replace the combination of a gravity accelerometer and a tilt sensor or the combination of three single accelerometer and gyroscopes in conventional wave buoys. After introducing the wave feature algorithm, high-precision and high-stability wave feature monitoring are achieved.

II. OVERALL DESIGN OF SIX-DIMENSIONAL ACCELEROMETER-BASED WAVE BUOY

A wave buoy has three components: the mechanical structure, the sensor system, and the system control module. 1) The stainless steel spherical buoy is equipped with lead-acid batteries, a control box (at the gravity center of the buoy control

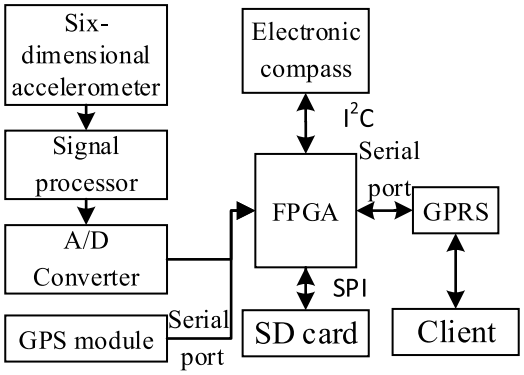

FIGURE 1. System diagram.

cabin, with a parallel six-dimensional accelerometer, a signal processor, a system controller, and other peripheral devices), and navigation lights. 2) The sensor system consists of a parallel piezoelectric six-dimensional accelerometer and a signal processor, collecting wave acceleration signals. 3) The system controller includes an FPGA processor, an A/D converter, a GPS module, a GPRS module, and a SD card to process, transmit, and save wave data. The buoy is also equipped with an electronic compass to collect the wave direction. The system diagram is shown in Fig.1.

The parallel six-dimensional accelerometer inside the buoy body moves with the wave. It exports wave-acceleration-related charge signals. These signals, which will be processed into effective voltage signals by the signal processor. Then the system uses dynamic modeling techniques and decoupling algorithm to obtain effective accelerations. The accelerations are integrated into speeds signals, which will be removed of the trend item and the effective speeds are obtained. The effective speeds are then integrated into the displacement signals, which will be removed of trend term. Finally, we have the effective displacement data.

Wave period and height can be obtained at the same time by applying zero-crossing process to Z-axis displacement. After the electronic compass gets angles, Kalman filtering is used to compute the main wave direction by merging the above-mentioned data with the acceleration sequences of the X and Y axes. The whole procedure is shown in the flow chart of Fig. 2.

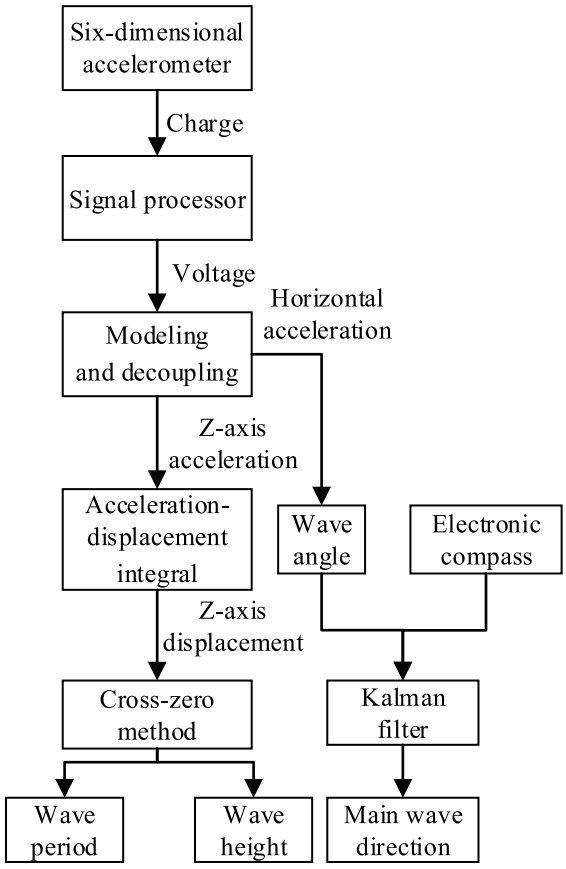

FIGURE 2. General flow chart of wave statistical algorithm.

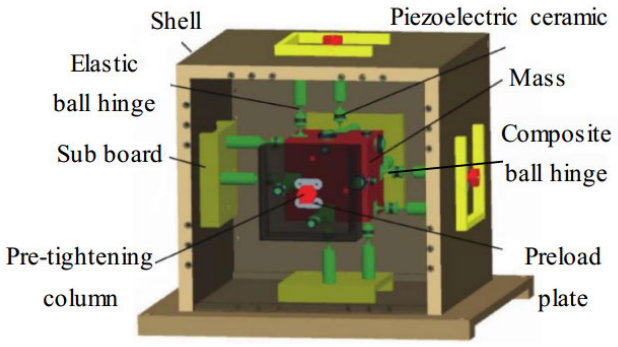

FIGURE 3. Digital prototype of Six-dimensional accelerometer.

III. HARDWARE DESIGN OF SENSOR SYSTEM

A. DESIGN OF ACCELEROMETER

The buoy system adopts a redundancy parallel structure with tetrahedral geometry of 12-SPS (12 is the number of branches, S represents the ball pair, and P the mobile pair). This structure is to form elastomer of the accelerometer [29], [30]. The digital and physical prototype of this new six-dimensional accelerometer is shown in Fig.3 and Fig.4, respectively. The six-dimensional accelerometer contains three parts, including 1) a mass, 2) a box-shaped outer casing (including four side plates, a bottom plate, and a top beam, all made of duralumin) and 3) 12 branches. The middle of each branch is a piezoelectric ceramic, and the two ends are elastic ball joints. The accelerometer has the advantages of large measuring range, high sensitivity, high precision and wide working frequency bandwidth.

The accelerometer consists of a mass, elastic ball hinges, piezoelectric ceramics, pre-tightening columns, preload plates, sub boards, and a shell. And it has one inertial mass and twelve identical branches. Each branch is formed by connecting a cylindrical piezoelectric ceramic and two elastic ball hinges located at both ends in series. The connection between the piezoelectric ceramics and the elastic ball hinges is by means of a conductive film and AB glue. One side of a

FIGURE 4. Physical prototype of six-dimensional accelerometer.

bare copper sheet of the conductive film is bonded to one electrode of the piezoelectric ceramic with AB glue, and the other side is bonded to the elastic ball hinge with AB glue. A wire is welded to the exposed copper sheet at the other end of the conductive film (the wire is connected to the signal processor through the M5 interface), so that the charges generated on the polarization surface of the piezoelectric ceramic can be derived. Each end of the piezoelectric ceramic is connected with an elastic ball hinge. The branches are equally divided into 6 groups (each two branched chains are one group), and the groups are vertically arranged with each other and share one composite ball hinge. Six composite ball hinges are respectively fixed on the midpoints of the upper rear edge, the upper left edge, the right rear edge, the lower front edge, the lower right edge, and the left front edge of the inertia mass. The other end of each branch is fixed on the sub board through an elastic ball hinge by using a positioning nut. Six sub boards are fixed by adjusting the pre-tightening columns (in the center of the boards) and the preload plates, so that the pre-tightening and anti-loosening of each branch chain are achieved. In addition, there are four through holes on the bottom plate, which make it easy to connect the accelerometer and the buoy control box firmly.

The specific parameters of the sensor are as follows:

Performance parameters: the working frequency is 0.1 Hz–100 Hz, and the range of linear acceleration is $-21.5g$ to $+21.5g$ (g is local gravitational acceleration), which meets the design requirements of ocean wave buoys. Specific dimensions: the side length of the cube inertial mass is 60 mm, the length of the inner large hinge is 55 mm, the length of the inner small hinge is 64 mm, the length of the outer hinge is 20 mm, the side length of the outer shell is 146 mm, and the total mass is 5.15 kg. In order to meet the requirements of rigidity and housing, the mass and pre-tightening screws are all made of ordinary steel, the shell is made of hard aluminum, and the elastic ball hinges are all made of elastic steel 65Mn. The flexible part of the elastic ball hinge is designed as an arc shape, in which the arc radius is 3 mm, the wide angle is 180°, and the minimum thickness is 1 mm. The selection of piezoelectric ceramics is PZT-5, P-51 series of lead zirconate titanate (PZT ceramics), which is cylindrical,

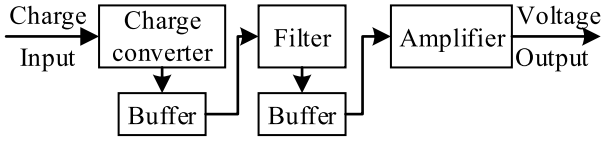

FIGURE 5. Structure of the signal processor.

with a bottom circle diameter of 5 mm and a thickness of 5 mm.

The accelerometer is fixed at the center of the buoy control box and the box is rigidly fixed at the center of the buoy shell. When the accelerometer senses the movement of the buoy, it will move with the ocean waves. The 12 branches will be compressed or stretched along with the mass under the action of inertial forces, and the piezoelectric ceramics will be subjected to corresponding axial forces [32], [33], which trigger the positive piezoelectric effect of the 12 ceramics and produce polarized charges. The electric charge (its amount and polarization) generated by each piezoelectric ceramic is proportional to the axial force it receives, and the proportional coefficient is the piezoelectric constant of the ceramic. According to the piezoelectric theory, the deformations of the branches are deduced. Moreover, the motion amount of the mass relative to the shell is calculated by the kinematics theory of the parallel structure. Therefore, the motion amount of the mass relative to the inertial reference system is calculated. Finally, the accelerations collected by the parallel six-dimensional accelerometer are obtained. At this time, the obtained accelerations are the accelerations of the buoy, which are the accelerations of the ocean wave.

B. DESIGN OF SIGNAL PROCESSOR

In order to reduce the influence of the accelerometer itself and external interference, a signal processor is designed. The signal processor processes charge signals output by the accelerometer to realize charge-to-voltage, reduce interference, and amplify the signals.

The signal processor includes a charge converter, two buffers, a filter, and an amplifier. Its inputs are charge signals output by the parallel six-dimensional accelerometer, and its outputs are voltage signals. The charge converter converts charge signals into voltage signals. The buffers coordinate, buffer, and isolate signals to improve signal quality. The filter removes the interference signals and retains the required signals. And the amplifier amplifies the signals and ensure that the range of the signals output by signal processor meets design requirements and prevent signal distortion. The schematic is shown in Fig. 5.

IV. WAVE STATISTICAL ALGORITHM

The voltage signals output from the signal processor will be processed by the FPGA processor. After applying dynamics modeling and decoupling algorithm to the signals, effective accelerations are obtained. The accelerations are integrated

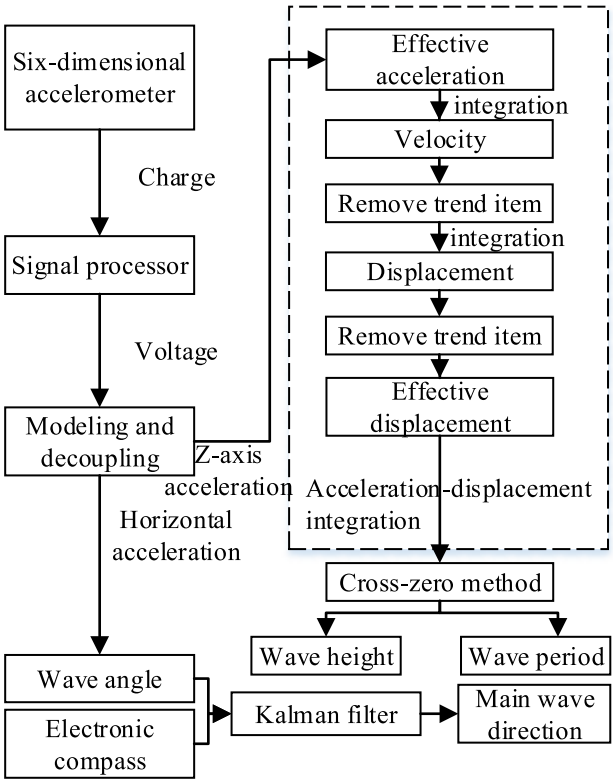

FIGURE 6. Detailed flow chart of wave statistical algorithm.

into speeds, which will be removed of the trend item to calculate the effective speeds. The effective speeds are integrated to obtain the displacements. The displacement signals are removed of trend item again to get effective displacement data.

The wave period and wave height can be obtained simultaneously by applying zero-crossing processing to Z-axis displacement sequences. Kalman filtering is used to compute the main wave direction by merging the angles obtained by the electronic compass and the acceleration sequences of the X and Y axes. The flow chart of the algorithm is shown in Fig. 6.

A. ACCELERATION DECOUPLING

During the study of parallel six-dimensional accelerometers, it is found that decoupling algorithm is crucial to the redundancy parallel 12-SPS structure with tetrahedral geometry. Therefore, how to improve the efficiency and adaptability of the algorithm is the core problem for the study. As the topological configuration of the sensor's elastomer determines the decoupling algorithm, designing a suitable parallel structure to be the elastomer will be the best option. The basic decoupling principle of the six-dimensional accelerometer is to estimate the accelerations of the shell relative to its inertial frame of reference. The estimation is based on motion parameters of the mass relative to the shell (including displacements, velocities, and accelerations). The upper and lower platforms of the parallel structure correspond to the mass and the pedestal (shell) of the six-dimensional accelerometer, respectively. Therefore, the kinematics feature of the parallel structure is an important standard for an appropriate elastic structure of the six-dimensional accelerometer.

The inputs of the parallel six-dimensional accelerometer are six independent components about the shell accelerations, and the outputs are the axial forces of the 12 branches. All outputs will change together with every input. Therefore, the accelerometer is a multi-input, multi-output, non-linear, and strongly coupled system. "Forward dynamics solution" is to deduce outputs from inputs via dynamic equations. On the contrary, "reverse dynamics solution" is to extrapolate inputs from outputs, also known as "decoupling". This paper uses the motion of the mass relative to the shell as a "bridge" to build a mathematical relation between six inputs and twelve outputs of the six-dimensional accelerometer. It has achieved full decoupling of the six-dimensional acceleration via the dynamic equations.

As lightweight piezoelectric ceramics have a very good rigidity and both ends are connected to the spherical pairs, the 12 branches can be seen as a two-force bar without deformation. Thus, the forces acting on the mass block include the axial force f_i (i is the branch number) and gravitational force mg, where m is the mass of the mass block and g is the local gravitational acceleration.

Here, the pre-matrix and post-matrix are in the form of:

$$\overset{+}{S} = \begin{bmatrix} s_0 & -s_3 & s_2 & s_1 \\ s_3 & s_0 & -s_1 & s_2 \\ -s_2 & s_1 & s_0 & s_3 \\ -s_1 & -s_2 & -s_3 & s_0 \end{bmatrix}. \tag{1}$$

$$\overset{-}{S} = \begin{bmatrix} s_0 & s_3 & -s_2 & s_1 \\ -s_3 & s_0 & s_1 & s_2 \\ s_2 & -s_1 & s_0 & s_3 \\ -s_1 & -s_2 & -s_3 & s_0 \end{bmatrix}. \tag{2}$$

The elements s_0, s_1, s_2, s_3 are real numbers, and the column vectors consisting of elements s_0, s_1, s_2, s_3 are recorded as S. Wherein, matrix with positive superscript ("+") is the pre-matrix, and that with negative superscript ("−") is the post-matrix.

The conversion relationship between the angular velocity vector ω and the attitude matrix R is:

$$\dot{R} = \begin{pmatrix} \hat{\omega} & 0 \\ 0^T & 0 \end{pmatrix} R. \tag{3}$$

where, $R = (\overset{-}{\Lambda})^T \overset{+}{\Lambda}$, $\overset{+}{\Lambda}$ is the pre-quaternion matrix and $\overset{-}{\Lambda}$ is post-quaternion matrix. They are matrices where the values of the elements of equation (1) and equation (2) are the real part q_0 and imaginary parts q_1, q_2, q_3 of quaternions respectively.

Two dynamic formulas of the parallel six-dimensional acceleration sensor system are derived by Newton-Euler

method:

$$\begin{pmatrix} a \\ 0 \end{pmatrix} = \frac{1}{m} R \begin{pmatrix} f_1 + f_3 - f_7 - f_9 \\ -f_4 + f_6 + f_{10} - f_{12} \\ -f_2 - f_5 + f_8 + f_{11} \\ 0 \end{pmatrix} + \begin{pmatrix} g \\ 0 \\ 0 \\ 0 \end{pmatrix} \tag{4}$$

$$\begin{pmatrix} \varepsilon \\ 0 \end{pmatrix} = \frac{3}{2mn} R \begin{pmatrix} f_5 - f_6 + f_{11} - f_{12} \\ f_1 - f_2 + f_7 - f_8 \\ -f_3 + f_4 + f_9 + f_{10} \\ 0 \end{pmatrix}. \tag{5}$$

In above formulas, n is the half-length of the mass edge, a is the three-dimensional linear acceleration vector, and ε is the three-dimensional angular acceleration vector.

Define

$$W = \left(\omega^T, 0\right)^T. \tag{6}$$

After combining the above-mentioned formulas (1) (2) (3) (6), it is obtained:

$$2\begin{pmatrix} \overset{+}{\dot{\Lambda}} \end{pmatrix}^T \overset{+}{\Lambda} + 2\begin{pmatrix} \overset{-}{\Lambda} \end{pmatrix}^T \overset{+}{\dot{\Lambda}} = \overset{+}{W} \begin{pmatrix} \overset{-}{\Lambda} \end{pmatrix}^T \overset{+}{\Lambda} - \overset{-}{W} \begin{pmatrix} \overset{-}{\Lambda} \end{pmatrix}^T \overset{+}{\Lambda}. \tag{7}$$

The multiplication of the pre-matrix and the post-matrix satisfies the commutative law:

$$\overset{+}{S}\overset{-}{S} = \overset{-}{S}\overset{+}{S}. \tag{8}$$

In addition, the pre-four-element matrix and the post-four-element matrix also satisfy:

$$\overset{+}{\Lambda}\begin{pmatrix} \overset{+}{\Lambda} \end{pmatrix}^T = \begin{pmatrix} \overset{+}{\Lambda} \end{pmatrix}^T \overset{+}{\Lambda} = \overset{-}{\Lambda}\begin{pmatrix} \overset{-}{\Lambda} \end{pmatrix}^T = \begin{pmatrix} \overset{-}{\Lambda} \end{pmatrix}^T \overset{-}{\Lambda} = E_4. \tag{9}$$

$$\overset{+}{\Lambda}\overset{-}{S}\begin{pmatrix} \overset{+}{\Lambda} \end{pmatrix}^T = \overset{-}{S}. \tag{10}$$

In formula(9), E_4 is a fourth-order identity matrix.

According to formulas (8) (9) (10), formula (7) is calculated as:

$$\begin{pmatrix} \omega \\ 0 \end{pmatrix} = 2\begin{pmatrix} \overset{-}{\Lambda} \end{pmatrix}^T \overset{\bullet}{\Lambda}. \tag{11}$$

And

$$\begin{pmatrix} \omega \\ 0 \end{pmatrix} = R\begin{pmatrix} \omega^* \\ 0 \end{pmatrix}. \tag{12}$$

Therefore, the following formula is derived:

$$\overset{\bullet}{\Lambda} = \frac{1}{2}\overset{*}{\Lambda}\begin{pmatrix} \omega^* \\ 0 \end{pmatrix}. \tag{13}$$

The first-order derivation of formula (12) is combined with formula (5) to obtain:

$$\begin{pmatrix} \dot{\omega} \\ 0 \end{pmatrix} = \begin{pmatrix} \hat{\omega} & 0 \\ 0^T & 0 \end{pmatrix} R\begin{pmatrix} \omega^* \\ 0 \end{pmatrix} + R\begin{pmatrix} \dot{\omega}^* \\ 0 \end{pmatrix}. \tag{14}$$

Since $\varepsilon = \dot{\omega}$, and according to formulas (9) and (14), it is obtained that:

$$\begin{pmatrix} \varepsilon \\ 0 \end{pmatrix} = \begin{pmatrix} \dot{\omega} & 0 \\ 0^T & 0 \end{pmatrix}\begin{pmatrix} \omega \\ 0 \end{pmatrix} + R\begin{pmatrix} \dot{\omega}^* \\ 0 \end{pmatrix} = R\begin{pmatrix} \dot{\omega}^* \\ 0 \end{pmatrix}. \tag{15}$$

Substituting the above formula into formula (4), the attitude matrix and formula (9) are arranged to obtain:

$$\dot{\omega}^* = \frac{3}{2nm} \begin{pmatrix} f_5 - f_6 + f_{11} - f_{12} \\ f_1 - f_2 + f_7 - f_8 \\ -f_3 + f_4 - f_9 + f_{10} \\ 0 \end{pmatrix}. \tag{16}$$

As $\dot{\omega}^*$ has a unique certain value at each sampling instant, it can be replaced by V: $\dot{\omega}^* = V$.

Thus, two first-order ordinary differential equations are derived via the trapezoidal method for the dynamic equations.

$$\omega^*_{(N)} = \omega^*_{(N-1)} + \frac{h}{2}\left(V_{(N-1)} + V_{(N)}\right). \tag{17}$$

$$\Lambda_{(N)} = \Lambda_{(N-1)} + \frac{h}{4}\overset{*}{\Lambda}_{(N-1)}\begin{pmatrix} \omega^*_{(N-1)} \\ 0 \end{pmatrix} + \frac{h}{4}\overset{*}{\Lambda}_{(N)}\begin{pmatrix} \omega^*_{(N)} \\ 0 \end{pmatrix}. \tag{18}$$

In above formulas, h is the acquisition step size of the output. The right subscripts (N) and $(N-1)$ respectively indicate the times N and $N-1$.

Since most carriers are changed from static to dynamic, the initial amount of auxiliary angular velocity is zero vector in general. In addition, in the initial state, the carrier coordinate system coincides with the inertial coordinate system, so:

$$\Lambda_{(0)} = (0, 0, 0, 1)^T. \tag{19}$$

Premultiply the above formula by $\overset{+}{\Lambda}_{(N)})^T$ to obtain:

$$\begin{pmatrix} \overset{+}{\Lambda}_{(N)} \end{pmatrix}^T a_{(N-1)} = \begin{pmatrix} -\frac{h}{4}\omega^*_{(N)} \\ 1 \end{pmatrix}. \tag{20}$$

In the formula, $a = (\alpha_1, \alpha_2, \alpha_3, \alpha_0)^T = \Lambda + \frac{h}{4}\overset{+}{\Lambda}\begin{pmatrix} \omega^* \\ 0 \end{pmatrix}$.

Swap the two terms on the left of equation (20) to get:

$$Q_{(N-1)}\Lambda_{(N)} = \begin{pmatrix} -\frac{h}{4}\omega^*_{(N)} \\ 1 \end{pmatrix}. \tag{21}$$

Of which, $Q = \begin{pmatrix} -\alpha_0 & -\alpha_3 & \alpha_2 & \alpha_1 \\ \alpha_3 & -\alpha_0 & -\alpha_1 & \alpha_2 \\ -\alpha_2 & \alpha_1 & -\alpha_0 & \alpha_3 \\ \alpha_1 & \alpha_2 & \alpha_3 & \alpha_0 \end{pmatrix}$.Its determinant is calculated as follows:

$$|Q| = -\left(a^T a\right)^2. \tag{22}$$

Decomposing formula (20) shows that a is not a zero vector. And matrix Q is nonsingular. Therefore, the nonhomogeneous linear equations of equation (21) have and only have one solution, as shown in equation (23).

$$\Lambda_{(N)} = \left(\frac{1}{a^T a}Q^T\right)_{N-1}\begin{pmatrix} -\frac{h}{4}\omega^*_{(N)} \\ 1 \end{pmatrix}. \tag{23}$$

The attitude matrix of the carrier relative to the inertial system is derived by substituting the formula above into the attitude matrix. The attitude matrix and the axial forces are substituted into equations (4) and (5) to obtain a unique array $\{a, \varepsilon\}$. So far, the full decoupling of the six-dimensional acceleration is completed [34]–[36].

B. ACCELERATION-DISPLACEMENT INTEGRAL ALGORITHM

After the decoupling, the effective accelerations are obtained. The next step is to acquire effective displacement sequence. This can be done through integrations and the removal of the trend item. It is based on the integral relationship of acceleration, velocity, and displacement. Compound trapezoid formula is adopted to perform the integration, and the trend item is removed to reduce errors during the acceleration-displacement integration [37], [38].

The acceleration-displacement integration is:

Define the acceleration signals in the z-axis direction as $a(j)$ $(j = 1, 2, \cdots, n)$, then the speed signals are:

$$\begin{aligned} v(i) &= v(i-1) + [a(i) + a(i+1)]/2f_s \\ i &= 1, 2, \cdots, n-1; v_0 = 0. \end{aligned} \tag{24}$$

Which contain primary trend items $\varepsilon(i/f_s) + \delta + v_0$.

The displacement signals are:

$$\begin{aligned} s(k) &= s(k-1) + [v(k) + v(k+1)]/2f_s \\ k &= 1, 2, \cdots, n-1; s_0 = 0. \end{aligned} \tag{25}$$

Which contain quadratic trend items:

$$\varepsilon(i/f_s)^2 + (\delta + v_0)(i/f_s) + (\eta + s_0). \tag{26}$$

In equations (17) and (18), v_0 is the initial velocity and s_0 is the initial displacement. In addition, parameter ε is the DC component generated by the accelerometer to collect the acceleration signals. Parameters δ and η are constants produced by parameter ε after the primary and secondary integration.

Define fitting polynomials as:

$$f_m(t) = \sum_{k=0}^{m} p_k t^k \in \emptyset. \tag{27}$$

where, coefficients p_k are the polynomial coefficients; $\emptyset$ is a set of functions consisting of polynomials less than $m(m \leq n-1)$times. The calculation of coefficients p_k needs to satisfy the following formula.

$$I = \sum_{i=0}^{n-1} [v_i - f_m(t_i)]^2 = \sum_{i=0}^{n-1} \left[v_i - \sum_{i=0}^{m} \left[p_k t_i^k \right] \right]^2 = \min. \tag{28}$$

Then:

$$\frac{\partial I}{\partial p_j} = 2 \sum_{i=0}^{n-1} \left[v_i - \sum_{i=0}^{m} \left[p_k t_i^k \right] \right]^2 t_i^j = 0. \tag{29}$$

To:

$$\begin{bmatrix} n & \sum_{i=0}^{n-1} t_i & \cdots & \sum_{i=0}^{n-1} t_i^m \\ \sum_{i=0}^{n-1} t_i & \sum_{i=0}^{n-1} t_i^2 & \cdots & \sum_{i=0}^{n-1} t_i^m \\ \vdots & \vdots & & \vdots \\ \sum_{i=0}^{n-1} t_i^m & \sum_{i=0}^{n-1} t_i^{m+1} & \cdots & \sum_{i=0}^{n-1} t_i^{2m} \end{bmatrix} \begin{bmatrix} p_1 \\ p_2 \\ \vdots \\ p_m \end{bmatrix}$$

$$= \left[\sum_{i=0}^{n-1} v_i, \sum_{i=0}^{n-1} v_i t_i, \cdots, \sum_{i=0}^{n-1} v_i t_i^m \right]. \tag{30}$$

Primary trend item is:

$$f_1(t) = \sum_{k=0}^{1} p_k t^k = p_1 t + p_0. \tag{31}$$

Of which,

$$t = i/f_s i = 0, 1, 2, fc, \cdots, n-1. \tag{32}$$

To:

$$\begin{bmatrix} n & \sum_{i=0}^{n-1} t_i \\ \sum_{i=0}^{n-1} t_i & \sum_{i=0}^{n-1} t_i^2 \end{bmatrix} \begin{bmatrix} p_0 \\ p_1 \end{bmatrix} = \left[\sum_{i=0}^{n-1} v_i, \sum_{i=0}^{n-1} (i/f_s) v_i \right]^T. \tag{33}$$

To:

$$\begin{aligned} p_0 &= \frac{\sum_{i=0}^{n-1} (i/f_s)^2 \sum_{i=0}^{n-1} v_i - \sum_{i=0}^{n-1} (i/f_s) \sum_{i=0}^{n-1} v_i}{n \sum_{i=0}^{n-1} (i/f_s)^2 - \left[\sum_{i=0}^{n-1} (i/f_s) \right]^2} \\ p_1 &= \frac{n \sum_{i=0}^{n-1} v_i - \sum_{i=0}^{n-1} (i/f_s) \sum_{i=0}^{n-1} v_i}{n \sum_{i=0}^{n-1} (i/f_s)^2 - \left[\sum_{i=0}^{n-1} (i/f_s) \right]^2}. \end{aligned} \tag{34}$$

Similarly, the quadratic trend item can be obtained.

$$f_2(t) = \sum_{k=0}^{2} p_k t^k = q_2 t^2 + q_1 t + q_0. \tag{35}$$

The effective accelerations are $v(i) - f_1(t)$, and the effective displacements are $s(k) - f_2(t)$.

C. WAVE STATISTICS

Wave data mainly includes wave height, direction, and period. This system adopts the method of downward zero-crossing to derive wave statistics [39]. The main sensors are a parallel piezoelectric six-dimensional accelerometer and an electronic compass.

The main goal is to count the wave height and period. Firstly, the average wave height of ocean wave is set to be zero-datum line. Secondly, continuously measure the data and label the adjacent lower span zero points in the system. Thirdly, calculate and record the wave height and period of two adjacent lower zero-cross points. Data need to be stored in a specified array. It should be noted that the elements of wave height are arranged according to certain rules (such as from small to large or the opposite). Finally, the maximum wave height H_{max}, the average wave height H_{mean}, the effective wave height $H_{1/3}$, and its corresponding wave periods are calculated. As for the wave direction, an electronic compass is used to correct the data: firstly, the acceleration sequences

TABLE 1. Technical parameters of wave sensor.

Parameters	Monitoring range	Precision	Resolution
Height	0.5–18m	Better than 2% × measured value	0.01m
Period	2–30s	±0.2s	0.1s
Direction	0–360°	±1.5°	0.1°

TABLE 2. Technical parameters of wave sensor.

Parameters	Specifications	Parameters	Specifications
Buoy Body Diameter	1.2m	Weight	83kg
Number of Batteries	3	Battery	Lead-acid
Operating Voltage	10.5–17VDC	Material	316 stainless steel

from X and Y axes are used to calculate the direction, which is further corrected based on results of the electronic compass. Secondly, both data are merged by Kalman filtering. In wave direction data fusion of the electronic compass and the accelerometer, linear Kalman filter is used. The system state variable is the wave direction. The deviation measured by the accelerometer is used as t he control input, and the measured value of the electronic compass is used as the system observation variable. Thirdly, the direction values are divided into 16 intervals and the frequencies of each direction in each interval are calculated. The direction angle with the highest frequency is the main wave direction.

V. EXPERIMENTAL VERIFICATION

A. TECHNICAL PARAMETERS

According to the *Seashore Observation Specification* [40], [41], a standard that specifies the items and technical requirements for seashore hydro-meteorological observation of coastal and island observation stations, when the wind speed or wave height reach a certain value (depending on the situation of sea areas), wave observation should be intensified to once in an hour. The buoy should be put in water deeper than 10 m, with flat ocean floor and without areas of rapid waters.

Specifications for wave height, period, and direction include:

Wave height(m): ± 10% for level I and ± 15% for level II.

Wave direction(°): ± 5° for level I and ± 10° for level II.

Wave period(s): ± 0.5s.

Hence, wave observation has been designed with following parameters:

1) TECHNICAL PARAMETERS OF WAVE SENSOR

2) TECHNICAL PARAMETERS OF WAVE SENSOR

Maximum wave height, 1/10 wave height, 1/3 wave height, average wave height; 1/10 wave height period, 1/3 wave height period, average wave height period; and main wave direction.

3) TECHNICAL PARAMETERS OF WAVE SENSOR

B. WAVE POOL EXPERIMENT

To test the wave observation buoy, two experiments were designed, including 1) a laboratory test and 2) a wave pool test. The design fully considered the demand of the experimental platform and the schedule. After the tests, the measured data were analyzed to evaluate the function and performance of the system.

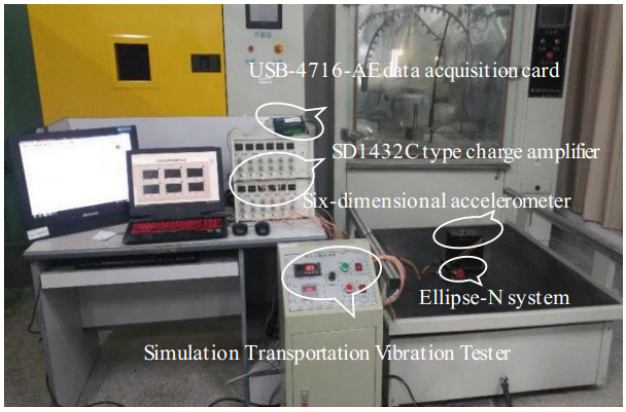

FIGURE 7. Acceleration test platform.

1) ACCELEROMETER TEST

An experimental platform is built to test the parallel piezoelectric accelerometer. The details are shown in Fig.7. The platform uses a Simulation Transportation Vibration Tester to simulate wave fluctuations. During the test, a parallel piezoelectric six-dimensional accelerometer and Ellipse-n system were placed on the tester. The tester was connected to an SD1432C charge amplifier. The data was collected by the USB-4716-AE data acquisition card and entered into the host computer for processing.

As can be seen from Fig. 8 (a), (b), and (c), the blue line in the chart is the output from the parallel piezoelectric accelerometer, and the red dotted line is the output from the Ellipse-n system. It can be observed that the acceleration signals from the two sensors are basically the same. It verifies the effectiveness and accuracy of the accelerometer.

2) WAVE POOL TEST

A wave pool is a pool in which there are artificially generated, reasonably random waves, like those of the ocean. By comparing the performance of both our buoy and the TRIAXYS MINI buoy in the wave pool, the accuracy and stability of newly designed buoy system have been proved. Fig. 9 shows the photos of this field-test.

According to the experiment, the average wave height, maximum wave height, 1/10 wave height, and 1/3 wave height derived by the system are in line with the results form of the TRIAXYS wave buoy. Detailed waveforms are shown in shown in Fig. 10(a)–(d). The system exported wave data every hour for 24 hours. The average wave height ranged from 0.15 m to 0.27 m, with the maximum wave height of 0.7 m. The results of wave height from our system overlapped those from the TRIAXYS MINI buoy, as can be shown

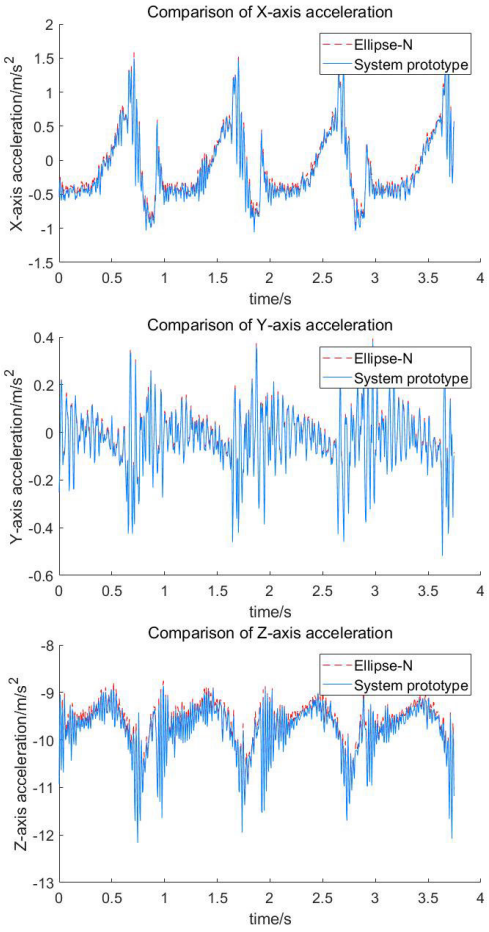

FIGURE 8. (a) is the comparison of X-axis acceleration, (b) is the comparison of Y-axis acceleration, and (c) is the comparison of Z-axis acceleration.

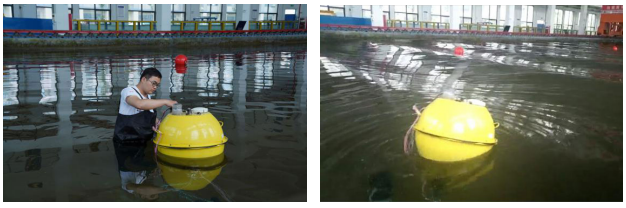

FIGURE 9. Wave pool experiment.

in the curve below. Hence, the system fully meets the design requirements in reality.

Fig. 11 shows the wave direction data observed by the system and the TRIAXYS MINI buoy. The wave period curves observed by the two buoys are basically the same. The wave directions were concentrated from 100° to 120°, and the direction with the largest frequency was about 112°. Therefore, the main wave direction was the ESE (east-southeast).

The comparison of parameters of the system and conventional wave buoys are shown in Table 3.

To conclude, the ocean wave observation buoy can accurately derive wave data during the observation period and it is able to successfully monitor the wave.

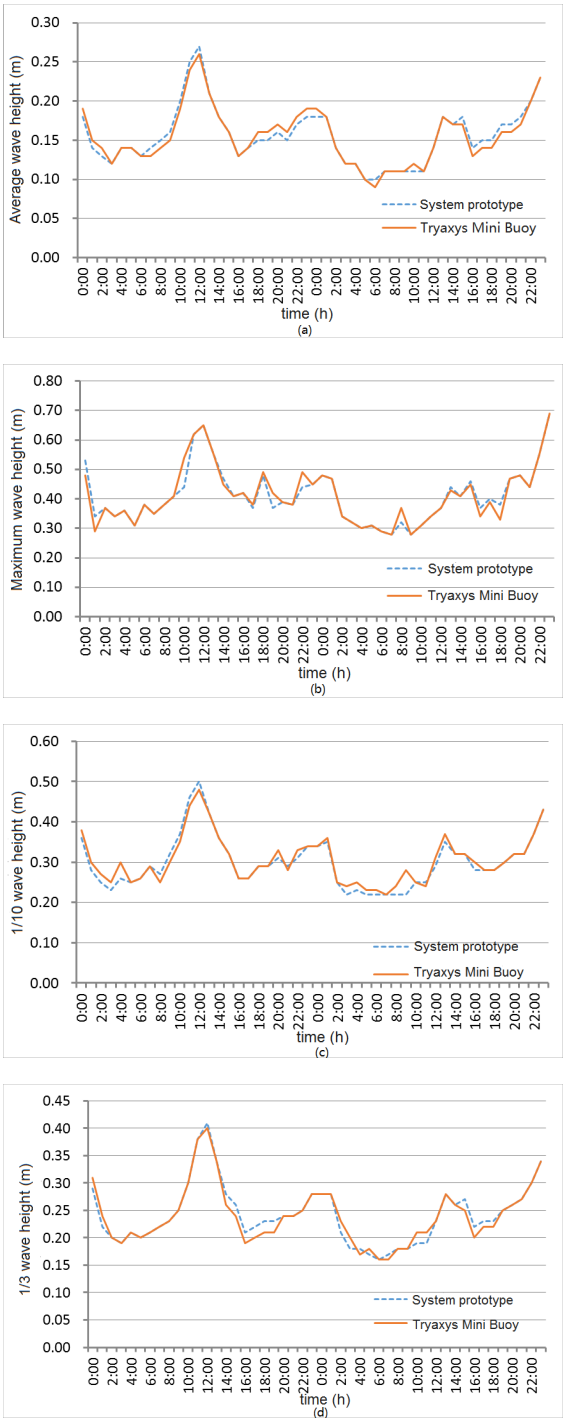

FIGURE 10. (a) is the average wave height, (b) is the maximum wave height, (c) is the 1/10 wave height, and (d) is the 1/3 wave height.

C. MARINE EXPERIMENT

Our observation site was around 1.33 kilometers away from the shore of Lianyungang Harbor, Jiangsu. Based on the onsite prospect, the water of the observation site was 10-meters-deep, with stable tide and silty sand, as can be shown in Fig. 12.

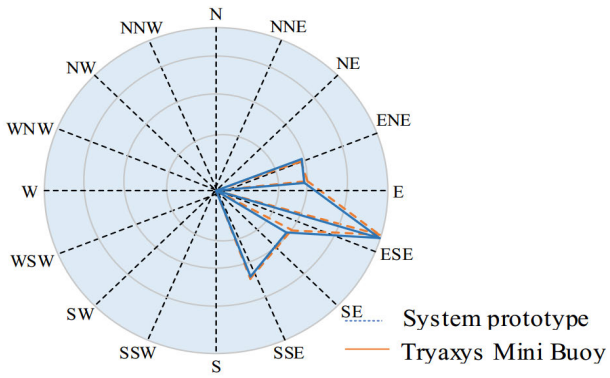

FIGURE 11. Ocean wave direction.

TABLE 3. Comparison of ocean wave observation buoys and conventional wave buoy parameters.

Parameters	Range	Accuracy	Buoy Manufacturer
Wave Height	±20m	2% × measured value	Datawell wave buoy
	0–20m	±(0.3 + 5% × measured value	SZF wave buoy
	0.3–20m	better than 3.75% × measured value	This system
Wave Direction	0–360°	±1.5°	Datawell wave buoy
	0–360°	±10°	SZF wave buoy
	0–360°	±1°	This system
Wave Period	1.6–30s	2% × measured value	Datawell wave buoy
	3–20s	±0.5s	SZF wave buoy
	2–30s	±0.3s	This system

FIGURE 12. Observation site.

1) METHOD

The wave buoy was used as an instrument to observe the ocean. The observation mode was ''regular observation'' (once an hour). The sampling interval was every 0.5 s.

2) DATA COLLECTION RATE

The data collection rate was 100%. It means that during the one-year investigation, the data were fully collected except during the replacement of the instrument.

The batteries of the instrument were changed for every three months. During the one-year observation, there were 28 groups of missing wave data. Since the missing waves were smaller than microwave, the influence is minimal.

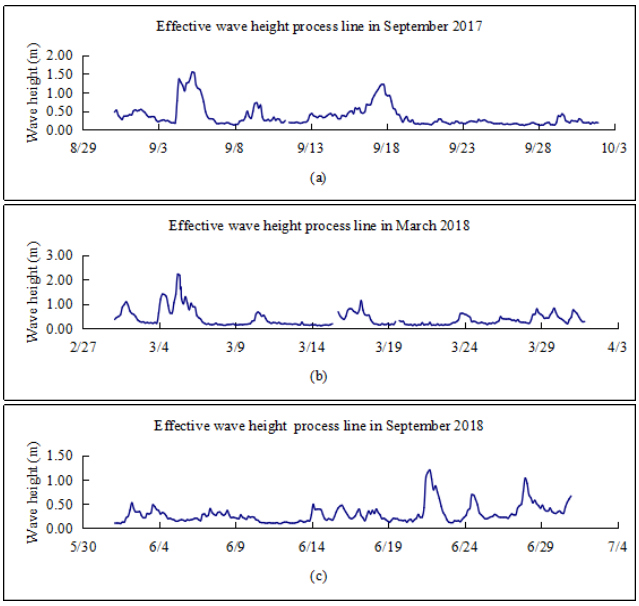

FIGURE 13. (a) is wave height in September 2017, (b) is wave height in March 2018, and (c) is wave height in September 2018.

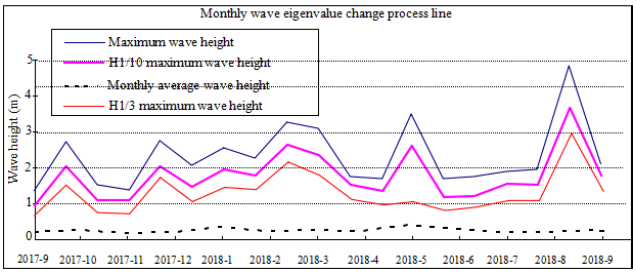

FIGURE 14. Monthly wave characteristic graph.

3) BASIC CHARACTERISTICS OF WAVES

From the one-year data observed, 3 months of wave height data from the total were selected to be shown in Fig. 13.

Fig. 14 shows the wave characteristic.

4) ROSE DIAGRAM

The 0–0.5 m wave rose diagram in March and December of 2017, as well as March and September of 2018 are shown in Fig. 15 (a)–(d). First, the number of main-direction waves was counted based on the total wave counts during the observation. Second, the numbers of waves in each direction were calculated, and categorized according to wave heights. Third, the frequency of waves in all directions within a certain height range was computed. The results are shown in wave rose diagrams, in which the main wave direction overlaps the maximum wave.

5) DATA ANALYSIS

Based on the analysis, more than 97.5% of the waves in the observation site were smaller or equal to level III (0.5–1.25m)

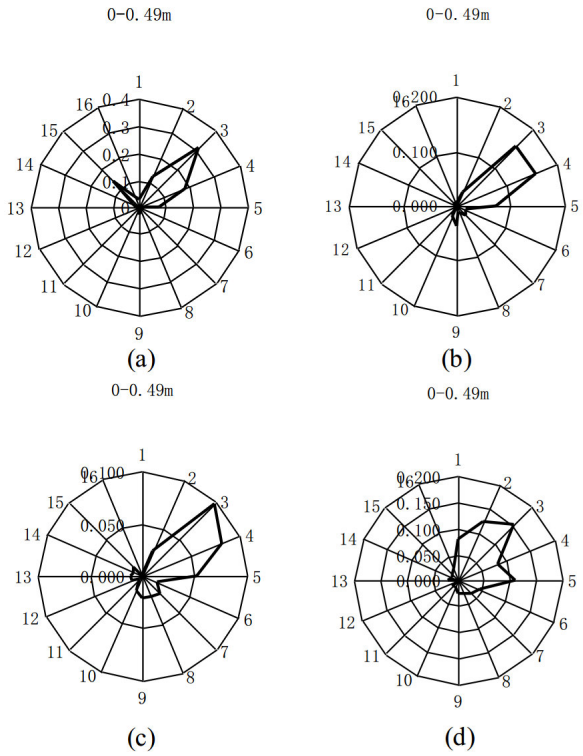

FIGURE 15. (a) is wave rose chart of September 2017, (b) is wave rose chart of December 2017, (c) is wave rose chart of March 2018, and (d) is wave rose chart of September 2018.

and there were more waves above level III in winter than in summer.

The main direction of waves below 0.5m in September and December of 2017 were respectively NE-ENE and NE-E; the waves of the same standard during March and September of 2018 concentrated in NE-ENE and E, respectively.

VI. CONCLUSION

Conventional wave observation method that combines the three-axis accelerometer-based wave sensor with the gyroscope show problems such as inner arm error, transverse sensitivity effect and gyroscope drift. Such problems will reduce data reliability of the system. This paper introduces a new type of parallel six-dimensional accelerometer that could be applied to the design of wave buoys. With a single mass and 12-chain redundancy added to the system, this kind of accelerometer reduces the principle error and improves stability and the method can be summarized as follows:

Firstly, the six-dimensional accelerometer was used to collect the electric charge data about wave accelerations. After the data had gone through the signal processor and FPGA processor, effective accelerations were modeled and decoupled. Next, the acceleration-displacement integral algorithm, which was adopted polynomial fitting to eliminate the trend terms. Moreover, integration algorithm of acceleration - displacement and zero-crossing method were applied to obtain the average wave height, the maximum wave height, the main wave direction, and other wave characteristics. After comparing high-precision sensors through experiments, we found that six-dimensional accelerometer was more accurate in wave height measurement than the 3.75 % $\times$ measurement value. It had wave direction accuracy of $\pm$ 1°, and the wave period measurement accuracy of $\pm$ 0.1s.

We are going to study marine environment monitoring in which unmanned ships, buoys and underwater robots are used together for the monitoring. The goal is to measure ocean waves and obtain meteorological information as comprehensively as possible.

REFERENCES

[1] T.-J. Chu, *Chinese Marine Data Buoy*. Beijing, China: Ocean Press, 2001.
[2] Q.-W. Zhou, S. Zhang, and H. Wu, "Overview of OceanWave observation technology," *Hydrographic Surveying Charting*, vol. ED-36, no. 2, pp. 39–44, Feb. 2016.
[3] S.-P. Zhang and J. Liang, "Development and application of hydrological telemetry system," *Ocean Technol.*, vol. 24, no. 4, pp. 5–7 and 13, Apr. 2005.
[4] *S4 Current Meter User Manual*, Inter Ocean Syst., San Diego, CA, USA, 1995.
[5] *SBE 26plus Manual*, Sea-Bird Electron., Washington, DC, USA, 1995.
[6] *Teledyne RDI's Workhorse Waves Array*, Teledyne Technol., Thousand Oaks, CA, USA, 2013.
[7] B. Robertson, Y. Jin, H. Bailey, and B. Buckham, "Calibrating wave resource assessments through application of the triple collocation technique," *Renew. Energy*, vol. 114, pp. 166–179, Dec. 2017.
[8] F.-Y. Wang, G.-N. Yuan, and Z.-Z. Lu, "Research progress of radar-based wave measurement technology at home and abroad," *Sci. Surveying Mapping*, vol. ED-33, no. 4, pp. 18–20, Apr. 2008.
[9] G.-Y. Wang, J.-P. Zhao, and R.-S. Song, "Estimation of wave extreme value using satellite microwave remote sensing data," *Port Eng. Technol.*, vol. 37, no. 1, pp. 14–21, Jan. 2000.
[10] J. Yang and J. Zhang, "Validation of sentinel-3A/3B satellite altimetry wave heights with buoy and Jason-3 data," *Sensors*, vol. 19, no. 13, p. 2914, Jul. 2019.
[11] H. E. Krogstad, S. F. Barstow, S. E. Aasen, and I. Rodriguez, "Some recent developments in wave buoy measurement technology," *Coastal Eng.*, vol. 37, nos. 3–4, pp. 309–329, Aug. 1999.
[12] G.-Y. Tang and Q. Kang, "Comparison of wave measurement methods with wave buoy," *Modern Electron. Technol.*, vol. ED-37, no. 15, pp. 121–122, 2014.
[13] C. V. Nelson and C. A. Keller, "Comparison between wave measurements using a wave spar buoy and an ENDECO type 1156, WAVETRACK buoy for winds less than 10 M/S: Preliminary data results," in *Proc. Ocean Technol. Opportunities Pacific (OCEANS)*, 1991, pp. 962–967.
[14] *The Directional Waverider DWR-MkIII: Over Three Years Continuous Operation*, Datawell B.V., Haarlem, The Netherlands, 2012.
[15] C.-C. Chen, J.-H. Zhu, and Y.-Q. Huang, "Reprocessing of wave knight data in the elevation effective wave height test," *Hydrographic Surveying Charting*, vol. ED-33, no. 3, pp. 53–55, May 2013.
[16] S. Barstow, G. Ueland, H. Krogstad, and B. Fossum, "The wavescan second generation directional wave buoy," *IEEE J. Ocean. Eng.*, vol. 16, no. 3, pp. 254–266, Jul. 1991.
[17] G.-Y. Tang and J.-P. Wang, "SZF wave buoy system," *Ocean Technol.*, vol. 27, no. 2, pp. 34–36, Feb. 2008.
[18] G.-Y. Tang, J.-Y. Zhou, and S.-W. L, "Development of 3M multiparameter wave buoy," *Meteorolog., Hydrolog. Mar. Instrum.*, vol. 36, no. 2, pp. 5–9, Feb. 2013.
[19] *TRIAXYS OEM Directional Wave Sensor USER'S MANUAL*, AXYS Technol., Sidney, BC, Canada, 2011.
[20] S. Naeth, D. Shumuk, and T. Ethier, "TRIAXYS G3 directional wave sensor," in *Proc. OCEANS MTS/IEEE Monterey*, Sep. 2016, pp. 1–9.
[21] J. Zhao, L. Hui, and S.-B. Chu, "Research on wave measurement technology based on triaxial acceleration," *J. Ocean Technol.*, vol. ED-34, no. 5, pp. 66–70, May 2015.

[22] J. Chae, H. Kulah, and K. Najafi, "A monolithic three-axis micro-g micromachined silicon capacitive accelerometer," *J. Microelectromech. Syst.*, vol. 14, no. 2, pp. 235–242, Apr. 2005.
[23] K. Okada, "Tri-axial Piezoelectric Accelerometer," in *Proc. Int. Solid-State Sens. Actuators Conf. (TRANSDUCERS)*, Aug. 2005, pp. 566–569.
[24] H. Takao, Y. Matsumoto, and M. Ishida, "A monolithically integrated three axial accelerometer using stress sensitive CMOS differential amplifiers," in *Proc. Int. Solid State Sens. Actuators Conf. (Transducers)*, Nov. 2002, pp. 1173–1176.
[25] B. Davis, "Using low-cost MEMS accelerometers and gyroscopes as strapdown IMUs on rolling projectiles," in *Proc. IEEE Position Location Navigat. Symp.*, Nov. 2002, pp. 594–601.
[26] Y. Suzuki and E.-B. Lin, "Current situation and trend of angular accelerometer," *Inertial Navigat. Instrum.*, vol. 1, no. 3, pp. 1–9, 1991.
[27] D. H. Wang and G. Yuan, "A six-degree-of-freedom acceleration sensing method based on six coplanar single-axis accelerometers," *IEEE Trans. Instrum. Meas.*, vol. 60, no. 4, pp. 1433–1442, Apr. 2011.
[28] J. W. Song and C. G. Park, "Optimal configuration of redundant inertial sensors considering lever arm effect," *IEEE Sensors J.*, vol. 16, no. 9, pp. 3171–3180, May 2016.
[29] C.-G. Li, J. Chen, and J.-J. You, "Fault diagnosis and repair of parallel six-dimensional accelerometer," *J. Vib. Shock*, vol. ED-36, no. 15, pp. 222–229, Jul. 2017.
[30] J.-J. You, "Research on piezoelectric six-dimensional acceleration sensor based on redundant parallel mechanism," M.S. thesis, Dept. Mechatron. Eng., NUAA Univ., Nanjing, China, 2013.
[31] J.-J. You, "Research on piezoelectric six-dimensional acceleration sensor based on 6-SPS parallel mechanism," Ph.D. dissertation, NFU, Tiddington, U.K., 2010.
[32] H.-Q. Zhai, C.-L. Cheng, and D.-B. Tang, "Model design of six-dimensional accelerometer," *Mechatronics*, vol. ED-17, no. 10, pp. 71–74 and 81, Oct. 2011.
[33] F.-L. Ni, P.-F. Lin, T. Zou, and D.-B. Tang, "Vibration suppression of flexible joints of large manipulators based on six-dimensional acceleration sensor," *Aerosp. Control Appl.*, vol. ED-44, no. 5, pp. 10–16, Oct. 2018.
[34] J.-J. You, C.-G. Li, and H.-T. Wu, "Hybrid decoupling and error self-compensation algorithm for parallel six-dimensional acceleration sensor," *Chin. J. Sci. Instrum.*, vol. ED-36, no. 10, pp. 2249–2257, Oct. 2015.
[35] J.-J. You, C.-G. Li, and H.-T. Wu, "Hamiltonian dynamics study of parallel six-dimensional accelerometer," *J. Mech. Eng*, vol. ED-48, no. 15, pp. 9–17, Aug. 2012.
[36] J.-J. You, Z.-Z. Fu, and C.-G. Li, "Decoupling parameter identification and disturbance analysis of parallel six-dimensional accelerometer," *J. Vib. Shock*, vol. ED-38, no. 1, pp. 134–141, Dec. 2019.
[37] F.-H. Zhou, Q. Xie, and D.-X. Wang, "Application of EEMD in detrended measurement in acceleration wave measurement technology," *Meteorolog. Hydrolog. Mar. Instrum.*, vol. ED-34, no. 02, pp. 77–82, Dec. 2017.
[38] G.-B. Wang, Y.-L. Liu, and X.-H. Jin, "Trend item processing based on the principle of least squares and its implementation of MATLAB," *Non-Ferrous Metall. Equip.*, vol. 19, no. 5, pp. 4–5, 2005.
[39] J. Zhao, "Wave measurement technology based on triaxial acceleration," *J. Ocean Technol.*, vol. ED-34, no. 5, pp. 66–70, Oct. 2015.
[40] *Specification of Coastal Observations*, State Ocean. Admin., Beijing, China, Sci. Press, 1987.
[41] Y.-L. Wu, "The new specification for seaside observations," *Mar. Forecasts*, vol. 5, no. 1, pp. 68–69, 1988.

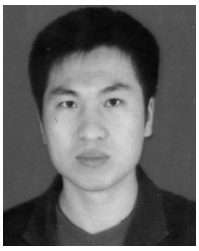

YUNPING LIU received the Ph.D. degree from the Nanjing University of Aeronautics and Astronautics, in 2009. He is currently an Associate Professor with the School of Information and Control, Nanjing University of Information Science and Technology. He is also the author of more than 20 journal articles. His current research interests include robotics, sensors, and multibody systems.

XIN WANG was born in Chengdu, Sichuan, China, in 1996. She received the B.S. degree in electrical engineering and its automation from the Nanjing University of Information Science and Technology, Jiangsu, China, in 2018, where she is currently pursuing the M.S. degree in control engineering. Her research interests include wave buoy, parallel mechanism, and acceleration sensor.

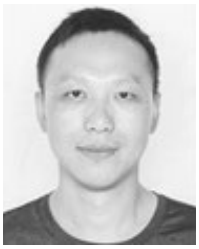

JINGJING YOU received the M.S. and Ph.D. degrees in mechanical and electrical engineering from the Nanjing University of Aeronautics and Astronautics, Nanjing, China, in 2010 and 2013, respectively.

He is currently an Associate Professor with Nanjing Forestry University. His research areas include parallel robot mechanism and six-axis accelerometer.

CHENG CHEN was born in 1991. He received the B.S. and M.S. degrees from the Nanjing University of Information Science and Technology, in 2014 and 2017, respectively. He is currently working with the Nanjing Automation Institute of Water Conservancy and Hydrology, Nanjing, China. His research interests include the rotorcraft navigation, tracking, stability, and robot.